Article

Epithelial restitution in 3D - Revealing biomechanical and physiochemical dynamics in intestinal organoids via fs laser nanosurgery

Intestinal epithelial restitution in 3D

Sören Donath,
Anna Elisabeth
Seidler, Karlina
Mundin, ...,
Alexander
Heisterkamp,
Manuela Buettner,
Stefan Kalies

donath@iqo.uni-hannover.de
(S.D.)
kalies@iqo.uni-hannover.de
(S.K.)

Highlights

Lesions in crypt bases of
colonoids are closed by the
flattening of adjacent cells

Epithelial cell layer
changes viscoelastic
properties during epithelial
restitution

Contractile forces of the
cytoskeleton are
indispensable for wound
healing

Single cell ablation in crypt
base leads to altered
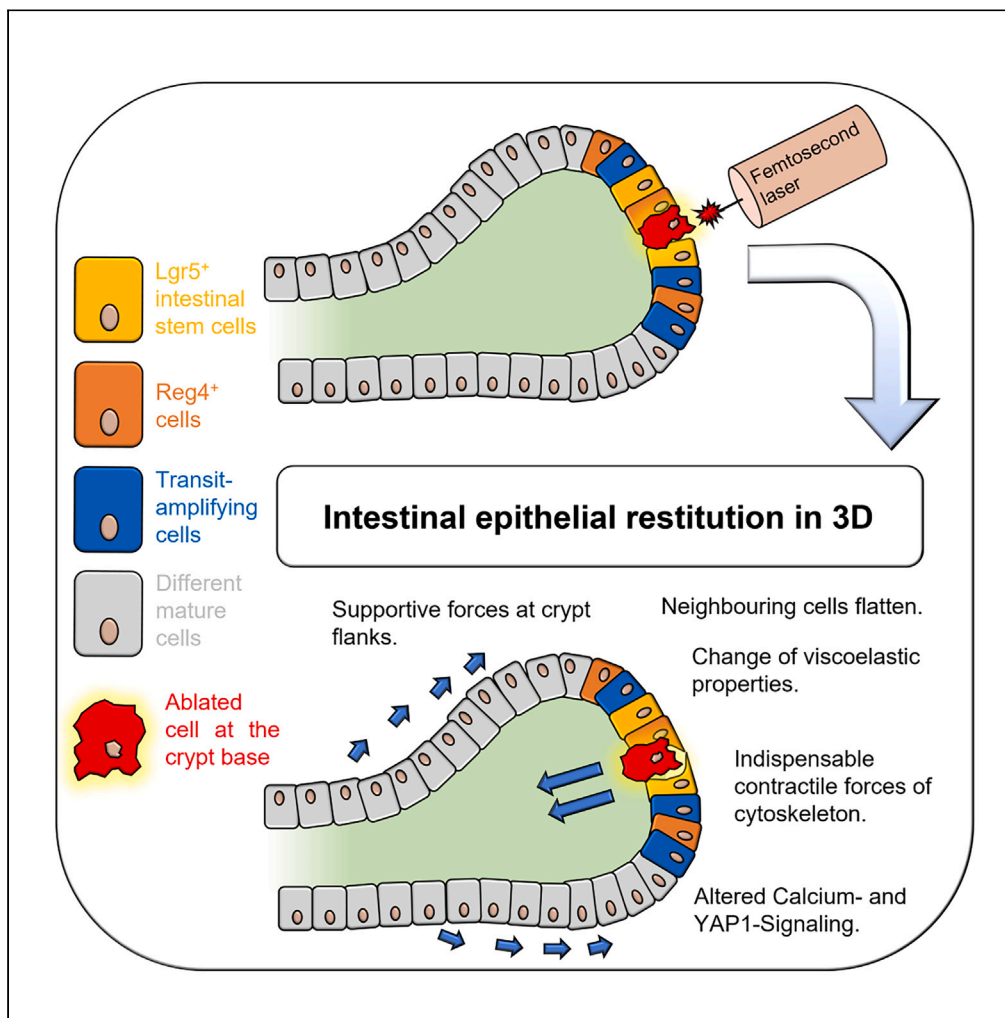Calcium- and YAP1-
signaling

iScience

Article

Epithelial restitution in 3D - Revealing biomechanical and physiochemical dynamics in intestinal organoids via fs laser nanosurgery

Sören Donath,[1,2,*] Anna Elisabeth Seidler,[1,2] Karlina Mundin,[1,2] Johannes Wenzel,[1,2] Jonas Scholz,[5] Lara Gentemann,[1,2,3] Julia Kalies,[1,2] Jan Faix,[5] Anaclet Ngezahayo,[6] André Bleich,[2,3,4] Alexander Heisterkamp,[1,2] Manuela Buettner,[2,3,4] and Stefan Kalies[1,2,3,7,*]

SUMMARY

Intestinal organoids represent a three-dimensional cell culture system mimicking the mammalian intestine. The application of single-cell ablation for defined wounding via a femtosecond laser system within the crypt base allowed us to study cell dynamics during epithelial restitution. Neighboring cells formed a contractile actin ring encircling the damaged cell, changed the cellular aspect ratio, and immediately closed the barrier. Using traction force microscopy, we observed major forces at the ablation site and additional forces on the crypt sides. Inhibitors of the actomyosin-based mobility of the cells led to the failure of restoring the barrier. Close to the ablation site, high-frequency calcium flickering and propagation of calcium waves occured that synchronized with the contraction of the epithelial layer. We observed an increased signal and nuclear translocation of YAP-1. In conclusion, our approach enabled, for the first time, to unveil the intricacies of epithelial restitution beyond *in vivo* models by employing precise laser-induced damage in colonoids.

INTRODUCTION

The integrity of the intestinal epithelial barrier is of pivotal importance for the maintenance of metabolism and homeostasis in mammals.[1–3] Individuals can face serious challenges upon barrier damage or disruption by pathogenic processes. For instance, disease patterns and lesions in the intestinal system can be caused by inflammatory bowel disease (IBD).[4] If a lesion is present within the epithelium of the gut, this can lead to an exchange of toxic and inflammatory factors between the luminal interior and the body, which can trigger uncontrolled immune reactions.[1,5,6] To prevent this, fast and effective restitution and regeneration are necessary. To investigate the repair and regeneration processes in such scenarios in detail, studies utilizing precise disruptions in the intestine need to be conducted.[7]

The intestinal barrier restoration can be divided into three processes. The transitions between these processes are seamless and cannot be strictly separated from each other (Figure 1).

The initial response of the intestinal system is epithelial restitution. Cells in the vicinity of the lesion flatten and migrate into the wound.[8] This closes the wound and partially restores the barrier within minutes to hours. To compensate for the loss of cells, increased the proliferation of the stem cells located in the crypts occurs. The resulting daughter cells migrate and differentiate along the crypt axis in the third phase of the repair process. Hence, tissue function and cell composition are completely restored. This article raises the question if similar repair processes occur in crypt damage.

Epithelial restitution represents the starting point and at the same time the underlying condition for all subsequent repair processes. To investigate this process further, colon-organoids, also called colonoids, can serve as a suitable cell culture model. Cultivated in a basement membrane matrix, their cellular composition and morphology better resemble the *in vivo* model than 2D *in vitro* cell culture models. Colonoids also represent the interactions of the different colon cell types, including stem cell-induced colon homeostasis.[7,9–11] In particular, these interactions play a crucial role in developing a profound understanding of the processes taking place upon epithelial damage. In the three-dimensional colonoid model, spatial as well as temporal information can be generated to elucidate these processes. To investigate

---

[1]Institute of Quantum Optics, Leibniz University Hannover, 30167 Hannover, Germany
[2]Lower Saxony Center for Biomedical Engineering, Implant Research and Development (NIFE), 30625 Hannover, Germany
[3]REBIRTH Research Center for Translational Regenerative Medicine, 30625 Hannover, Germany
[4]Institute for Laboratory Animal Science, Hannover Medical School, 30625 Hannover, Germany
[5]Institute for Biophysical Chemistry, Hannover Medical School, 30625 Hannover, Germany
[6]Institute of Biophysics, Leibniz University Hannover, 30167 Hannover, Germany
[7]Lead contact
*Correspondence: donath@iqo.uni-hannover.de (S.D.), kalies@iqo.uni-hannover.de (S.K.)
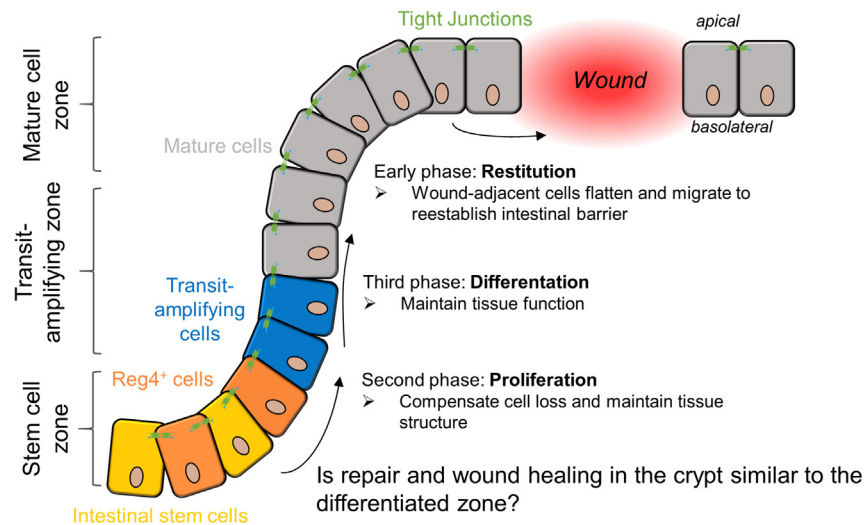https://doi.org/10.1016/j.isci.2023.108139

Figure 1. The three phases of wound healing in the intestine

To close lesions and avoid contact of luminal content with the basal lamina, neighboring cells flatten and migrate into the wound during epithelial restitution. Following, to replenish the cell loss, increased proliferation occurs, generating new cells via the intestinal stem cells. These cells migrate and differentiate along the crypt axis in the third phase.

the processes occurring during epithelial restitution, the study was always performed at a defined site, the crypt base, in order to be able to investigate associated biochemical and biophysical characteristics in the stem cell niche during damage as well.

To understand the precise initiation and progression of restitution events, we have recently established a colonoid wounding model, which involves the targeted laser-based ablation of individual or multiple cells in the colonoid crypt.[12] Such precise manipulation can hardly be achieved by ionizing radiation or treatment with various chemical components. Instead, we employ a femtosecond laser system leading to non-linear optical interactions with the investigated tissue and allowing for precise removal of (sub-)cellular structures.[12,13] This process, called femtosecond laser nanosurgery, is based on the creation of a low-density plasma of free electrons, produced mainly by multiphoton ionization.[14,15] As the process involves no significant heating, no thermal or mechanical energy is released in neighboring cells.[15,16] Thus, the combination of nanosurgery and live imaging enables the precise tracking of epithelial restitution, mechanosensitive answers, and mechanotransducive reactions. These data can be generated using the colonoid model to study epithelial restitution.

Various studies showed in two-dimensional cell layers that upon loss of single epithelial cells, the neighboring cells flatten, bringing the apical side into close spatial proximity to the basolateral cell side.[17,18] This is based on an excessive reorganization of the cytoskeleton, in particular, the cell's actin structures, and allows the rapid and efficient migration of cells into the lesion.[19,20] New cell-cell and cell-ECM contacts are formed and the cells change the ratio of their axes back to the ratios that exist during homeostasis within the intestinal tissue. Via our colonoid wounding model, we can extend this data using temporal recordings of restitution in a three-dimensional setting. We combine the wounding with the use of fluorescently labeled colonoids, genetically modified via lentiviral transduction, allowing for studying cell shape and position. In particular, the fusion protein occludin-mEmerald is expressed at the tight junctions and the basolateral membranes of the cells.[21,22] With the application of the deep learning algorithm Cellpose,[23,24] automated cell segmentation and tracking of cell morphology (cell size, cell perimeter, and cell-aspect ratio) are achieved. To further study the integrity and structure of the cellular epithelial layer after damage, we apply optical elastography via Brillouin spectroscopy.[25]

During the epithelial restitution process, forces are exerted at positions along the crypt axis to rapidly close the lesion. In our model, the utilization of traction force microscopy (TFM) allows for the observation and measurement of the involved forces. We track the displacement of fluorescent beads in the basement membrane extract (BME) after single-cell ablation using confocal microscopy. Image data were analyzed using TFMLab,[26] which calculates forces in three dimensions using free-form deformation.[27,28]

While the general architecture and symmetry of the colonic crypts have a notable impact on the exerted forces and the restitution process, it is also crucial to investigate the cytoskeleton and its primary component filamentous (F)-actin at the single-cell level.[18] The dynamic actin reorganization during epithelial damage is necessary to enable cell migration through the formation of cellular forces.[29–33] The filamentous structures interact with myosin 2 to form a contractile ring around the damaged cells.[18,34] The damaged cells are shed into the lumen and neighboring cells migrate in the direction of the lesion. To better understand these processes in our model, we applied different cytoskeletal inhibitors. Blebbistatin inhibits actomyosin-based contractility and thus cell motility by binding the myosin II head domain, greatly slowing down the release of phosphate and thereby stabilizing myosin in an F-actin unbound state.[35] Lantruculin B was used to depolymerize the F-actin network and cytochalasin D was added to inhibit actin polymerization.[36,37]

The reorganization of the cytoskeleton, is closely connected to calcium signaling, which is crucial in epithelial restitution.[38,39] For instance, *in vivo* photodamage of murine stomach epithelia was followed by a fast increase of extra- and intracellular Ca^{2+}-ions in cells near the wound site. The gastric restitution was impaired when these calcium concentration changes were inhibited.[39] Acute injury of the intestinal epithelium led to increased Ca^{2+} influx which was based on the activation of the transient receptor potential cation channel 1 (TRPC1).[40,41] In general, calcium signaling is connected to many pathways, including the activation of small GTPases such as RhoA and Rac1, to actomyosin-based contraction via calmodulin and to calpains, which dissociate various cytoskeletal connection points at the leading edge of a migrating cell.[42–45] Therefore, we aimed to use calcium imaging and inhibition to analyze the occurrence of calcium events during epithelial colonic restitution. We established a GCaMP5 biosensor to visualize calcium signaling in live cell imaging in response to damage to the colonoids and homeostatic conditions.[46]

To further reveal biomechanical signals during epithelial restitution, we investigated the potential activation and nuclear localization of the primary mechanical sensor of the cellular microenvironment YAP.[47] YAP activation in the colon leads to the increased attachment of epithelial cells to the extracellular matrix, increased epithelial cell movement, stem and progenitor cell expansion, and differentiation suppression.[48,49] Visualization and localization of YAP signaling via immunostaining were used to investigate the influence of wounding in the crypt base.

In summary, our study aims to recapitulate epithelial restitution via precise damage application and live cell imaging in a three-dimensional setting using femtosecond laser-nanosurgery. For the first time, this combination is used for measuring cellular morphology changes, exerted forces, and the involvement of actin, calcium signaling, and YAP.

RESULTS

Cells adjacent to the lesion change their morphology and migrate into the wound

Precise ablation of a single cell at the base of the crypts was used to investigate the mechanisms and forces occurring during epithelial intestinal restitution in the three-dimensional colonoid-wounding model. Occludin-mEmerald was used to visualize the exact cell outlines and Cellpose[24] served for cell segmentation. This allowed us to acquire the morphological parameters of cell size, cell perimeter, and cellular aspect ratio.

Ablation at the crypt base did not lead to a significant change in cell size, independent of the distance of the cells to the damaged cell (Figure 2B). The cell perimeter of neighboring cells located directly above the ablation site (0 μm) decreased significantly after 60 min, whereas further distant cells exhibited no perimeter changes (Figure 2A). In contrast to the cell area and perimeter, the cellular aspect ratio was strongly altered in cells close to the lesion site. The ratio of the directly adjacent cells, as well as those cells at a distance of up to 20 μm, decreased significantly (Figure 2C). The cells flattened and migrated into the wound, causing a shortening of the cellular major axis, while the minor axis was slightly stretched. The wound was closed as a result of stretching and flattening, although the cellular aspect ratio remained constant within the time frame of 90 min. The cell polarity was maintained during the process as indicated by the immunostaining of the vasodilator-stimulated phosphoprotein (VASP, Figure S1). VASP is a component of focal adhesions and acts as an anchoring point of F-actin on the basal cell side.[50,51] The basal ends of the adjacent cells stretched and associated with each other, and the apical side of the cells also stretched to the point of basal association. After the lesion is closed and the epithelial barrier is restored, the previously stretched cells return to their original morphology (Figure S1F).

The viscoelastic characteristics of the epithelial cell layer are not fully restored within the time frame of epithelial restitution

To analyze the impact of restitution on the viscoelastic properties of the cell layer, the restitution and subsequent reorganization of the epithelium were examined by Brillouin microscopy. A lesion in the epithelium led to a decrease in the Brillouin peak and consequently to a decrease of the longitudinal modulus and the correlated stiffness (Figure 3A). Up to a point in time of approximately 120 min, the Brillouin shift deviated from the initial shift. When the initial restitution and closure of the epithelium were completed at this time, the original architecture of the cell layer was not yet regained. Only after an extended time of 4 h, the shift corresponded to the homeostasis-conditioned shift.

Traction force microscopy reveals lower forces at the crypt sides and strong forces at the lesion upon its closure

Traction force microscopy was performed to investigate the exerted forces after single-cell ablation. Via TFMLab,[26] evaluation was performed using 1 μm red fluorescent beads in Cultrex BME at a dilution of 1:100 in Occludin-mEmerald positive colonoids.

The maximum force in response to single-cell ablation was observed shortly after damage at cells near the lesion (Figure 4A). We could distinguish traction forces at the ablation site in the direction of the lumen and traction forces at the flanks of the crypt, which acted away from the crypt and angled slightly toward the crypt base. The magnitude of the forces decreased with the distance from the lesion site (Figure 4B). In total, the depth-averaged forces in the time frame of up to 5 min at the lesion were approximately 30 Pa, with single positions reaching up to 210 ± 60 Pa. Those at the side of the crypt were approximately 17 Pa with single positions reaching up to 120 ± 20 Pa. Over time, both forces decreased sharply and remained constant after approximately 20 min as the damaged cell had been repelled into the lumen and the forces approached those under normal conditions.
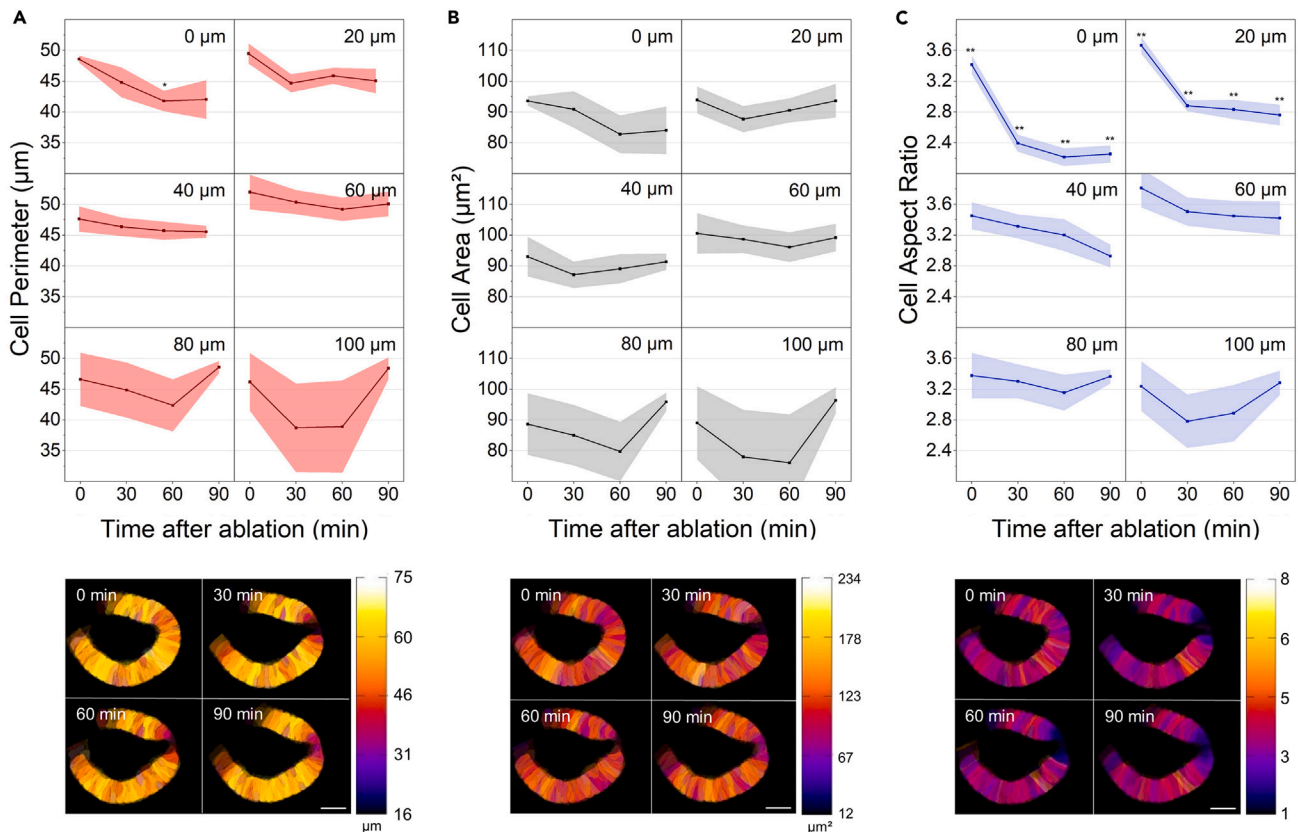
Figure 2. The process of epithelial restitution in the base of the colonic crypts changes the cellular aspect ratio of directly adjacent cells, while cell area and perimeter remain constant

Cell morphology (area, perimeter, aspect ratio) was investigated after single-cell ablation in occludin-mEmerald colonoids. Cells at a distance of 0 µm, 20 µm, 40 µm, 60 µm, 80 µm, and 100 µm from the ablation site were grouped and analyzed every 30 min. The upper panel shows the quantitative course of the measured parameters, and the lower panel illustrates an exemplary crypt (z-projection). The color coding corresponds to the measured parameter.

(A) The cell area does not change significantly.

(B) After 60 min, the perimeter of cells in the direct vicinity of the ablation site changes.

(C) A significant decline in cellular aspect ratio occurs in cells near the ablation site. Over time, the cellular apical axis becomes longer and the lateral axis shorter. Data from seven separate single-cell ablations were evaluated. The area around the evaluated measurement points in the upper panel represents the standard error of the mean (SEM). Scale bar corresponds to 25 µm. See also Figure S1.

Manipulation of actomyosin-based cell motility and inhibition of actin polymerization prevent restitution after single-cell ablation

The cytoskeleton, in particular, F-actin, has a great influence on the viscoelasticity of biological samples.[52] Therefore, various components of the cytoskeleton were destabilized and/or depolymerized, and epithelial restitution as well as the regeneration of the intestinal epithelial layer after single cell ablation were investigated. Single-cell ablation in the crypt area is indicated by a strong increase in autofluorescence of the destroyed cell.[12] Upon the application of 100 µM blebbistatin, an inhibitor of actomyosin-based cell mobility, the spatial extent of autofluorescence remained identical over time (Figure 5A) and the damaged cell mass was not pulled into the lumen of the colonoid, which was observed in untreated controls (Figure S2). While the crypt survived the lesion in the epithelium for 120 min, a total loss of structural integrity of the crypt and whole colonoid occurred after approximately 270 min. Controls treated with blebbistatin without laser ablation kept their structural integrity during this time frame (controls in the right panel of Figure 5).

Afterward, actin polymerization was inhibited via the application of 1 µM latrunculin B, which prevents the binding of G-actin to already existing F-actin.[36] The lack of attachment of new actin monomers results in the depolymerization of pre-existing F-actin structures. Under these conditions, single-cell ablation in the crypt led to its rapid dilation (Figure 5B). The colonoids were unable to close the lesion in the epithelial layer and fully lost integrity shortly after the failure of restitution. The occludin-mEmerald-related fluorescence signal was no longer correctly localized and became blurry, another indicator of degrading cells.

To validate whether already formed F-actin is sufficient to implement the reorganization of cellular structures needed for restitution, the inhibitor cytochalasin D (10 mg/mL) was used (Figure 5C). It binds to the growing F-actin end and prevents the new binding of G-actin as well as the depolymerization of existing actin filaments. We observed that single-cell ablation in the crypt region could not be regenerated
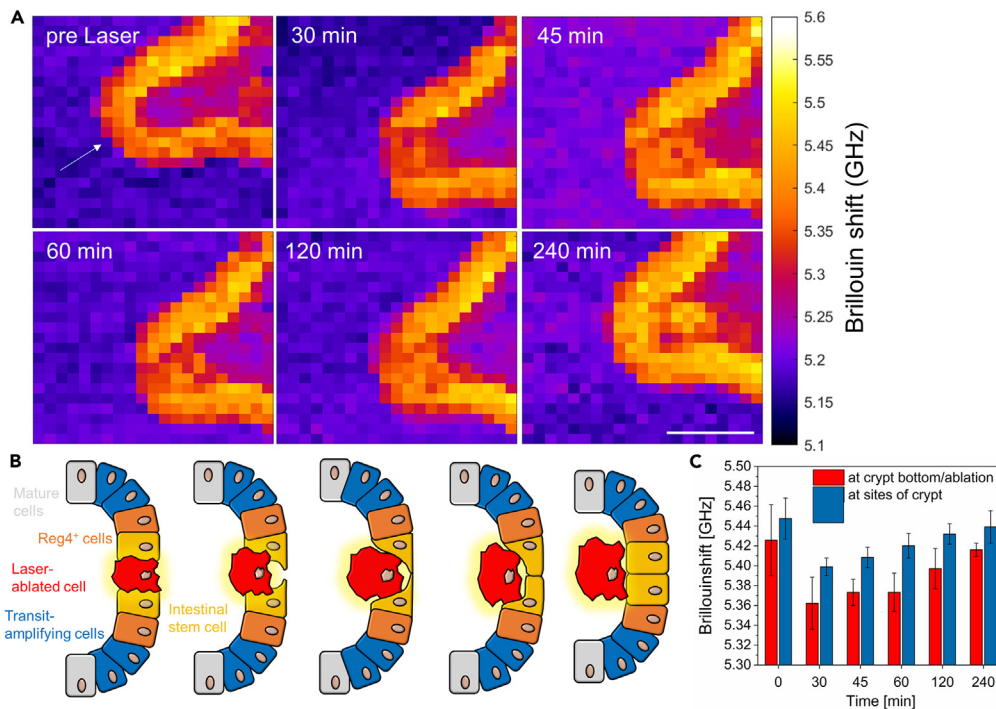
Figure 3. The viscoelastic characteristics of the epithelial cell layer are not completely restored within the time frame of epithelial restitution

(A) Single-cell ablation was performed in the base of the colonoid crypts and the time course of the Brillouin shift was subsequently examined. The damaged cell mass is recognizable by a deviating Brillouin shift, shed into the lumen, and the cell layer is restored. The Brillouin shift of the epithelial layer is not restored immediately after closure of the barrier but requires an extended period of 240 min. The study was performed on three single cell ablation scenarios. The scale bar corresponds to 50 μm.

(B) Schematic temporal course of epithelial restitution in the crypt base. The ablated cell is pulled into the lumen, and the cells adjacent to the lesion stretch into the lesion, closing the intestinal barrier.

(C) Time course of changes in Brillouin shift after single-cell ablation. Brillouin shifts were determined in a region of interest of 50 μm at the crypt base and at both sides of the crypts. Values from the two crypt sides were averaged. Data from three ablation scenarios were measured, SEM is plotted as error bars.

by pre-existing f-actin. In contrast to latrunculin B, the crypt was not dilated after damage, and structural integrity was kept for about 300 min (Figure 5C).

Damage at the crypt base leads to calcium flickering in adjacent cells and calcium waves correlating with epithelial contraction

The transmission of mechanosensitive (stress-related) signals is coordinated by a complex network, which also includes calcium signaling.[53–55] To investigate epithelial calcium signaling in the three-dimensional colonoid-wounding model, a lentiviral GCaMP5 sensor was used.[46] Immediately after cell ablation, a high-frequency flickering of the calcium-induced fluorescence signal (Video S1) occurred at the basolateral site of lesion-adjacent cells that underwent the strongest morphological changes (see Figure 2C). After about 30 min, calcium waves were detected, transmitted from the direction of the crypt base and the lesion toward the differentiated epithelium (Figure 6A). In addition to this early calcium wave, we also observed signals which were potentially no longer associated with the initial damage-related reaction. Figure 6B shows a wave spreading from the lesion toward the differentiated epithelium after 120 min. These late calcium waves were accompanied by a strong contraction of the epithelium (Figure 6C and Videos S2 and S3). If intracellular calcium was chelated by BAPTA, the crypt was no longer able to close the generated wound. The damaged cell was not pulled into the lumen but was deposited in the BME on the basal cell side (Figure S3).

YAP/TAZ signaling is activated in lesion-adjacent cells

Calcium is capable of transmitting a variety of signals, whereby mechanosensitive signals can be converted into biochemical reactions. One pathway that can be activated by calcium signaling in response to mechanical stress is the Hippo pathway.[56] As YAP/TAZ are the primary mechanical sensors of the cellular microenvironment,[47] these two interactors have multiple roles after epithelial damage. Based on the essential role of YAP in epithelial regeneration, YAP expression and localization in response to single-cell ablation were investigated by immunostaining. Colonoids were fixed and stained 30 min after ablation. An increased YAP signal was detected in cells surrounding the lesion (Figure 7). This signal was more localized to the nucleus but was also increased in the cytoplasm across the nuclear borders compared to controls.
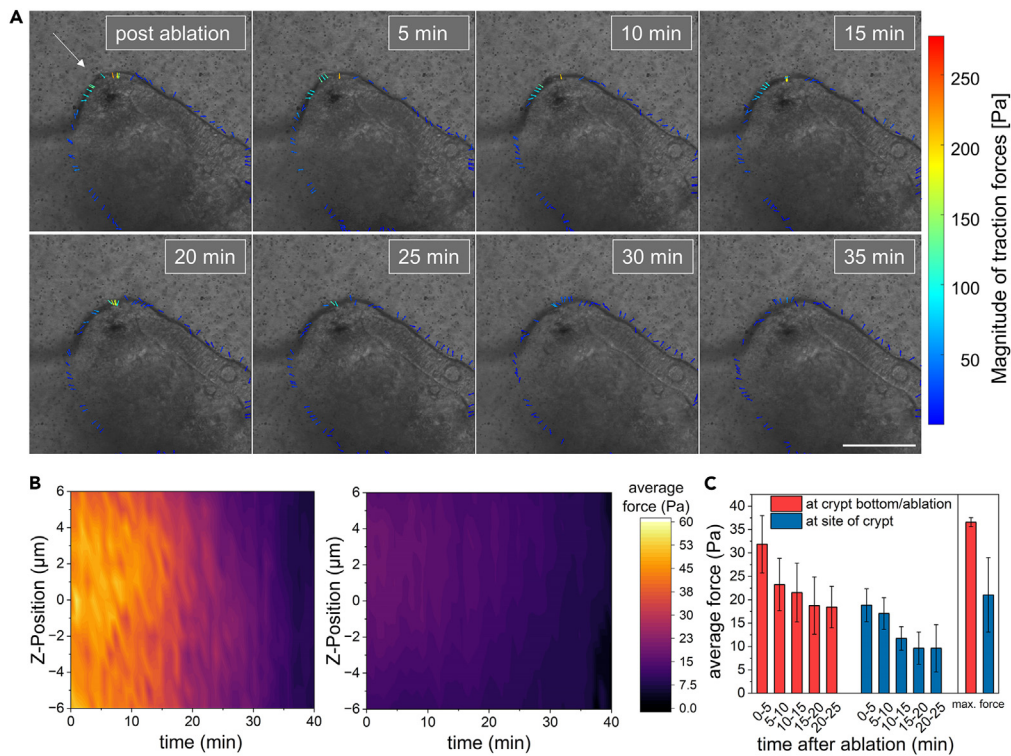
Figure 4. Forces acting at the lesion and crypt flanks during epithelial restitution in the colonoid crypts

(A) Time course of the traction forces during epithelial restitution. The ablation position is indicated by a white arrow. The largest forces act on the lesion immediately after ablation, directed toward the lumen. Smaller forces can also be detected on the sides of the crypts, acting away from the crypt, slightly angled toward the base of the crypt. The scale bar corresponds to 50 μm.

(B) Time course of force in different planes at the crypt base (left) and the crypt flanks (right). Both positions show a radial progression from the ablation plane to more distant z-positions, with the average force being more pronounced at the crypt base and a decrease of the forces over time.

(C) Spatially averaged forces at the crypt base and crypt side. N = 6 single cell ablation scenarios, the standard error of the mean (SEM) is depicted.

As in ablated crypts, a progression of the YAP-associated signal away from the crypt base could also be seen in control crypts, but the signal in control crypts was much less pronounced than around lesions (Figure S4).

DISCUSSION

An intact intestinal barrier is of pivotal importance for the entire mammalian organism. The study of the interactions of cells during barrier homeostasis and damage, e.g., in pathologies, requires novel methods that go beyond conventional 2D *in vitro* cell culture. On the one hand, *in vivo* animal experiments are adequate to better understand various underlying mechanisms and cellular interactions of multiple tissues. But on the other hand, in order to limit animal experiments following the 3R principle[60,61] and focus on the regenerative capacity and autocrine of only the epithelia, organoid systems represent an excellent alternative tool. Due to the organoids' mimicry of *in vivo* cell types and interactions, questions can be clarified that would hardly be accessible with other cell culture models, for instance, epithelial restitution and the cell interactions during this process in the intestine.

In the colon, the process of re-establishing the epithelial barrier upon damage is not yet clarified. Targeted ablation of individual cells in colonoids can provide a better understanding of repair and regenerative processes, which includes the initial processes of epithelial restitution in this area. We aimed to address this issue using femtosecond laser nanosurgery for targeted cell damage in this study, focusing on the visualization and investigation of various aspects of the epithelial restitution of lesions.

Closure of the lesions requires the extensive reorganization of the cytoskeleton, in particular of f-actin.[62,63] Intra- and intercellular signals are processed via cell-cell junctions, creating a network of interacting cell neighbors.[64,65] If these cell-cell junctions are interrupted by a lesion, the reaction of the surrounding cells in a three-dimensional model is of great interest. It was observed that the neighboring cells stretched toward the lesion. We assume that the coordinated rearrangement and reorganization of F-actin for cell stretching and migration into the wound leads to a shift in the cellular aspect ratio. The changes in morphology likely serve to form a contractile actomyosin cable at the wound ends, which has been demonstrated in various other epithelia.[62,66–72] This cable, which serves to transport the damaged cell mass into the lumen of the colonoid on the apical cell side, could also be observed in our study: Cellular actin structures associate at the basal side with VASP (Figure S1), which participates as an adherent junction protein in the (re)assembly of F-actin by locally enhancing actin
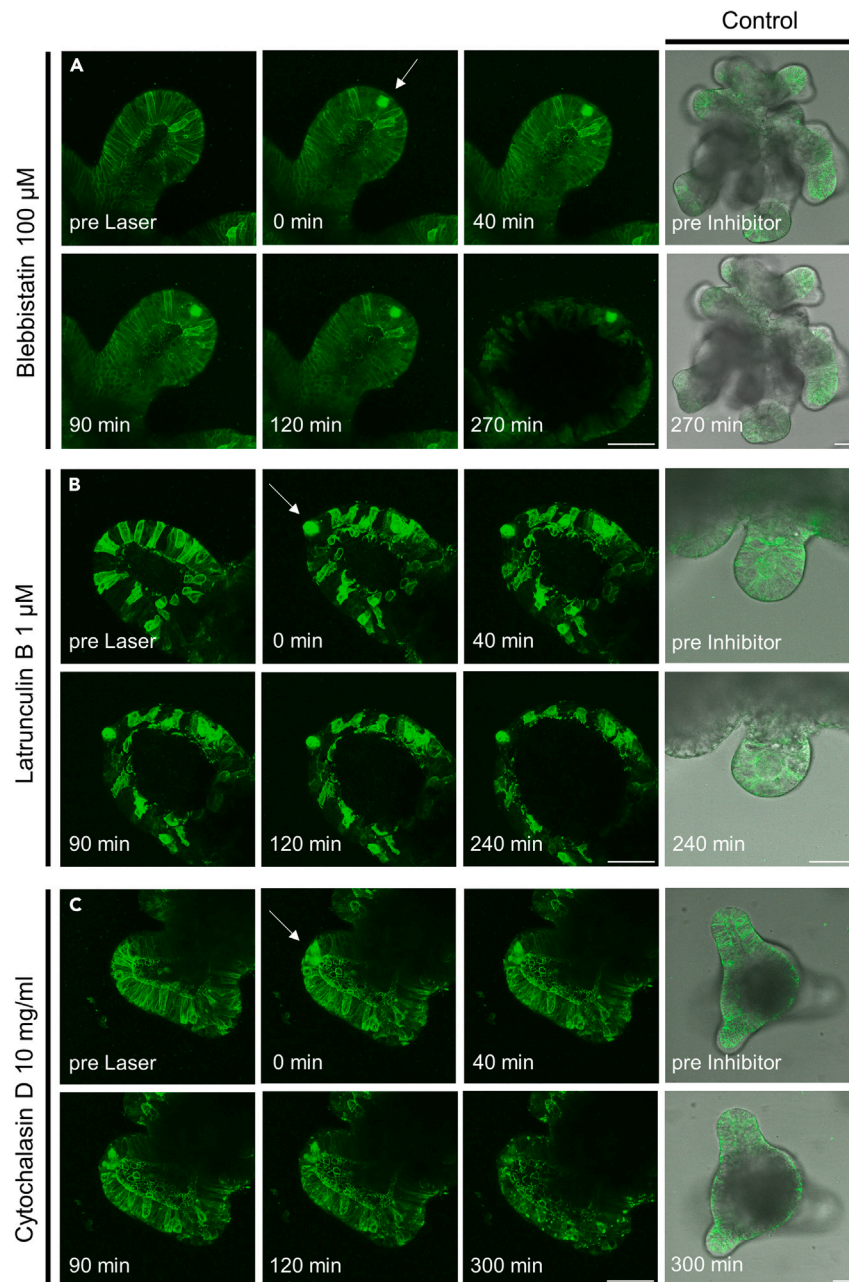
Figure 5. Inhibition of acto-myosin-based cell motility (blebbistatin), depolymerization of f-actin structures (latrunculin B), and prevention of attachment of new g-actin monomers (cytochalasin D) lead to the prevention of epithelial restitution

(A) Single-cell ablation in the crypt base is indicated by a strong autofluorescence signal from the ablated cell. The neighboring cells are unable to shed the destroyed cell material into the lumen of the colonoid upon the addition of 100 μM blebbistatin. The crypt loses integrity after 270 min.

(B) Upon the addition of 1 μM latrunculin B, the destroyed cell material is neither pulled into the lumen nor is the lesion closed. The crypt dilates significantly and loses integrity within 2 h.

(C) Inhibition with 10 mg/mL cytochalasin D leads to blockage of the attachment of monomeric g-actin monomers to existing F-actin structures. The pre-existing structures are unable to close the lesion, the destroyed cell remains in its position and the crypt loses integrity. Single-cell ablation is indicated by a white arrow in each case. Controls without laser ablation are shown in the right column, showing intact and correctly localized occludin-mEmerald based fluorescence. Time points correspond to laser ablation. Laser ablation was done 30 min after incubation with the respective inhibitor.N = 4 single cell ablation scenarios per experimental condition, the scale bar corresponds to 50 μm. See also Figure S2.
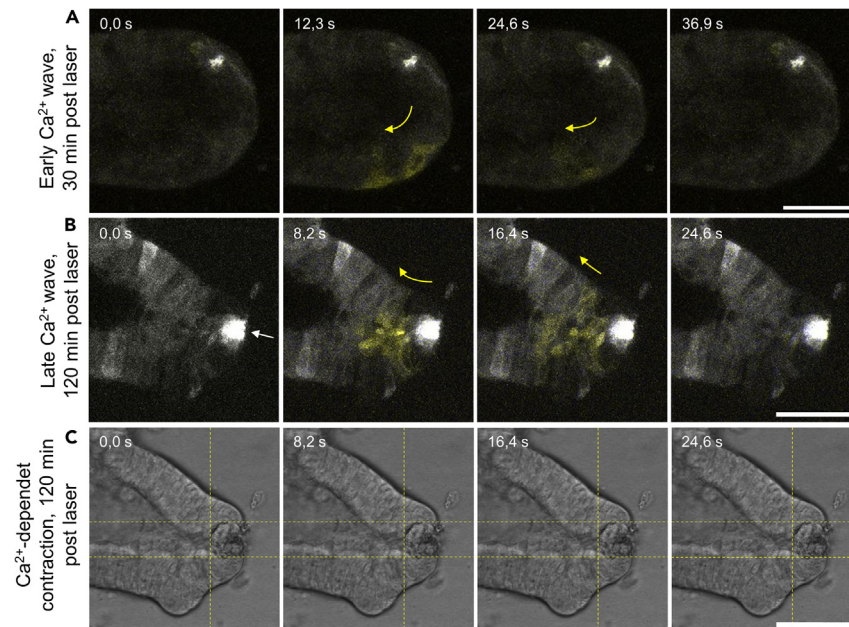
Figure 6. Intercellular Ca²⁺ waves are detectable during the regeneration processes and induce contractions of the colonic epithelium

Lentivirally transduced GCaMP5 colonoids were femtosecond laser-damaged at the crypt base.

(A) An intercellular Ca²⁺ wave, visualized by binding to the calcium indicator GCaMP5 is transmitted from the ablation site along the epithelium 30 min after laser-ablation and during the early phase of regeneration.

(B) Radial propagation of a strong calcium spark from the lesion 120 min after laser-ablation in CMV-GCaMP5 colonoids in medium with 10 mM CaCl₂. A contraction of the epithelium around the lesion is observed in conjunction with the calcium spark (C). Crypts in Figures A and B are shown as z-projections (confocal microscopy, (A) 20 μm depth, z-step size 4 μm; (B and C) 9 μm depth, z-step size 3 μm; (A and B) Z projection max intensity of green fluorescence signal); in Figure C, the crypt is shown in one z-plane as a transmitted light image and the yellow dashed lines serve for orientation. White arrows indicate the ablation site, and yellow arrows the direction of propagation of the calcium waves. Scale bar corresponds to 50 μm. Figures A, B, and C are shown in supplementary movies 1, 2, and 3. See also Figure S3 and Videos S1, S2, and S3.

polymerization.[73–75] The VASP staining showed the bending of cells next to the lesion and early association of the basal ends. The apical ends of the cells were shifted to the basal side, thereby changing the cellular aspect ratio, which was restored after the completion of restitution.

The inhibition of different cytoskeletal constituents and interactors demonstrated the importance of a functional F-actin apparatus for epithelial restitution. The inhibition of actomyosin-based cell motility by blebbistatin led to the inhibition of the removal of the damaged cell mass. The myosin II-dependent contractility could no longer be realized,[76,77] whereby the gap in the epithelium remained such that the damaged crypt lost integrity after some time. A similar result was seen when the F-actin structures were directly affected. If existing F-actin structures were depolymerized and the formation of new structures was prevented by latrunculin B, wound healing was also inhibited. Upon the blockage of the association of globular actin monomers with pre-existing F-actin by cytochalasin D, the damaged crypt was also unable to close the lesion. Therefore, we can hypothesize that in response to the damage, newly polymerized F--actin is required for wound healing and the formation of the contractile cable, which pulls the damaged cell mass into the lumen. Consequently, the term "reorganization" of the cytoskeleton, which is often used in the context of epithelial restitution, could be extended to "new-organization" of the cytoskeleton in lesion-neighboring cells.

The loss of integrity of the crypts might be distinguished in the three different cases of inhibition. Latrunculin B causes the complete dissolution of the F-actin structures leading to the direct destruction of the crypts after single-cell ablation. In the other two cases, existing F-actin structures remain unaffected, and the crypt can withstand dilation for an extended period. Additionally, the potential side effects of the inhibitors should not be disregarded. We were able to show that the colonoids survive the treatment of the inhibitors without laser damage, but it is evident based on the morphology that the individual substances influence the cytoskeletal structures of the cells (Figure 5, right panel). For example, Pentinmikko et al. showed that the inhibition of non-muscular myosin 2 strongly affects apical contact traction, the shape of intestinal stem cells, and signaling pathways of cells located in the crypts.[78] In addition, the measurement of viscoelasticity during epithelial restitution using Brillouin microscopy in our study showed that further rearrangements occur within the neighboring cells in addition to the initial closure of the barrier (Figure 3A). We assume that after the damaged cell has been shed into the lumen, the altered actin structures in the neighboring cells (schematically shown in Figure 3B) get back to their normal status.

Upon the application of all actin inhibitors, the damaged cell mass was never shed into the lumen. This may be attributed to the absence of contractile forces. The crypts could no longer provide the required forces. Our investigation using traction force microscopy indicated the forces necessary in the uninhibited case (Figure 4). Here, the largest average force acted directly at the lesion in the direction of the lumen,
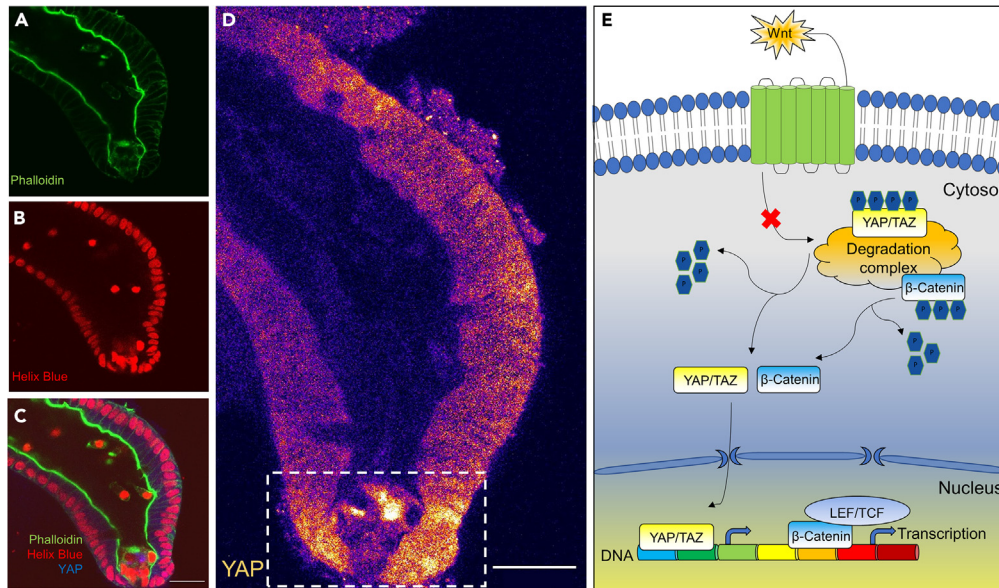
Figure 7. Single-cell ablation in the crypt base leads to increased YAP signal in the surrounding cells
To show the localization and expression of YAP1, a lesion was created and the colonoid was fixed and immunostained 30 min after ablation.
(A) Phalloidin staining (phalloidin-Atto 488, Sigma Aldrich, St. Louis, MO, USA) to visualize the F-actin structures within the crypts.
(B) Helix Blue Staining (Helix NP Blue, Biolegend, San Diego, CA, USA) was used for the visualization of the cell nuclei.
(C) Merge of phalloidin-488, Helix Blue, and YAP1 staining.
(D) YAP1 staining indicates the expression and localization of YAP1 within the damaged and restituting crypts. The region of interest is marked with a dashed line.
5 single cell ablation scenarios were evaluated and immunostained.
(E) Interplay of the Wnt and Hippo-YAP/TAZ pathways. When the Wnt pathway is active, YAP/TAZ is released from the degradation complex. TAZ degradation depends on the phosphorylation of β-catenin.[47,57] β-catenin can escape the degradation complex when Wnt is active, translocates to the nucleus, and initiates the transcription of various genes via interaction with LEF/TEF.[47,58] Based on the escape of β-catenin, YAP/TAZ translocates into the nucleus and activates Wnt/β-catenin-dependent transcription.[47,59] Scale bar corresponds to 25 μm. See also Figure S4.

most likely provided by the contractile actomyosin ring. In addition to this force, which decreased in the radial and temporal course, additional forces occurred at the sides of the crypts, although with a much smaller magnitude. These forces were exerted in the direction of the crypt base and are most likely necessary to support the migration and stretching of neighboring cells into the lesion (Figure 2C).

Since actomyosin-based contractility is dependent on the myosin light-chain kinase and calmodulin, and thus on calcium signaling,[43,44] we aimed to investigate calcium signaling during the restitution process. We could exemplarily observe an early calcium wave at about 30 min after single-cell ablation, which moved away from the damage site. In addition, another wave could be identified at a later timepoint (exemplarily approx. 2h after ablation), which also propagated away from the damage site. It is known that epithelial restitution requires the mobilization of endogenous calcium.[39,79] Furthermore, very rapid calcium flickering in neighboring cells could be shown (Video S1), which is in agreement with several studies investigating the dependence of cell migration on (intra-)cellular calcium during restitution.[79,80] Due to the rapid variation of calcium concentration and the new organization of the cytoskeleton, the cells can quickly change their shape and close the wound.[29] If this signal transmission is blocked by the chelation of intracellular calcium with BAPTA,[39] we observed that neighboring cells were no longer able to close the wound (Figure S3). The calcium waves were shown to be associated with a contraction of the intestinal epithelium (Figure 6C and Videos S2 and S3). This contraction could be the result of coordinated contraction triggered by the transmission of the calcium signal from cell to cell. This could represent a mechanism of coordinated force application to close the lesion at the crypt base. Due to the shortness of this contraction, it might not have been possible to resolve it using traction force microscopy.

We could previously show that single-cell ablation in the crypt area leads to increased Wnt signaling.[12] Via Wnt activation at the frizzled receptor, a short calcium pulse occurs.[81] Based on this interaction between Wnt and calcium and the direct interplay between Wnt and the primary sensor of the cellular microenvironment YAP/TAZ,[47,82] Hippo YAP/TAZ signaling was verified to be activated after ablation via YAP1 immunostaining. In general, YAP1 signaling decreased from the crypt base to the differentiated area.[47,83,84] 30 min after ablation, the YAP1 signal was strongly increased in cells near the lesion (Figure 7D). YAP might fulfill further roles than its mechanosensitivity. The ablation might lead to a translocalization of YAP1 from the cytoplasm into the nucleus, to trigger stem cell expansion and differentiation inhibition.[47–49] Additionally, the overall increased expression, compared to control crypts, may be due to the release of YAP1 in combination with β-catenin from the destruction complex (Figure 7E).[58]

In summary, the combination of three-dimensional colonoids, live cell imaging using genetically fluorescently labeled colonoids, and single-cell ablation via a femtosecond laser system allowed us to generate, for the first time, highly resolved insights into the process of colon

epithelial restitution. This was complemented by further advanced techniques such as Brillouin microscopy and traction force microscopy. Our wounding model allows precise and cell-specific damage that cannot be achieved via treatment with chemicals or ionizing radiation. Further experiments and results can be generated via the system, which can shed light on a deeper understanding of pathological, but also homeostasis-related processes within the intestinal system. For instance, in future studies, patient cells might be used to investigate genetic disorder-associated influence on colon wound healing with this model.

Limitations of the study

In this study, some limitations should not be ignored.

First of all, it should be considered that organoids were cultured from different mice and vary depending on the age and sex of the mouse. Furthermore, the organoids themselves also show differences depending on the cultivation time, which could not be completely eliminated. Furthermore, the influence on various barrier properties by lentiviral overexpression of the fluorescent protein of mEmerald and occludin should be considered.

In general, organoids represent an excellent improvement over standard *in vitro* cell culture systems, but they should still be further characterized in terms of transferability of gained results to the *in vivo* model.

STAR★METHODS

Detailed methods are provided in the online version of this paper and include the following:

- KEY RESOURCES TABLE
- RESOURCE AVAILABILITY
  - Lead contact
  - Materials aviability
  - Data and code aviability
- EXPERIMENTAL MODEL AND STUDY PARTICIPANT DETAILS
  - Isolation of colonic crypts and growth of colonoids
- METHOD DETAILS
  - Colonoid culture and transduction
  - Nanosurgery setup, manipulation, and imaging of colonoids
  - Analysis of cell morphology
  - Optical elastography via Brillouin microscopy
  - Traction force microscopy
  - Immunostaining
- QUANTIFICATION AND STATISTICAL ANALYSIS

SUPPLEMENTAL INFORMATION

Supplemental information can be found online at https://doi.org/10.1016/j.isci.2023.108139.

AUTHOR CONTRIBUTIONS

Conceptualization, S.D. and S.K; methodology, S.K.; software, J.W., K.M., and S.K.; validation, S.D., A.E.S., L.G., J.W., and S.K.; formal analysis, S.D. and S.K.; investigation, S.D., A.E.S., J.W., K.M., J.S., J.K., J.F., and S.K.; resources, J.K., M.B., and S.K.; data curation, S.D., J.W., K.M., A.N., M.B., and S.K.; writing—original draft preparation, S.D. and S.K.; writing—review and editing, all authors; visualization, S.D. and S.K.; supervision, S.K.; project administration, A.B., A.N., A.H., M.B., and S.K.; funding acquisition, A.B., A.H., and S.K. All authors have read and agreed to the published version of the article.

DECLARATION OF INTERESTS

The authors declare no competing interest.

iScience
Article

CellPress
OPEN ACCESS

REFERENCES

1. Sturm, A., and Dignass, A.U. (2008). Epithelial restitution and wound healing in inflammatory bowel disease. World J. Gastroenterol. *14*, 348–353. https://doi.org/10.3748/wjg.14.348.

2. Nusrat, A., Delp, C., and Madara, J.L. (1992). Intestinal epithelial restitution characterization of a cell culture model and mapping of cytoskeletal elements in migrating cells. J. Clin. Invest. *89*, 1501–1511. https://doi.org/10.1172/JCI115741.

3. Beumer, J., and Clevers, H. (2016). Regulation and plasticity of intestinal stem cells during homeostasis and regeneration. Dev *143*, 3639–3649. https://doi.org/10.1242/dev.133132.

4. Okamoto, R., and Watanabe, M. (2005). Cellular and molecular mechanisms of the epithelial repair in IBD. Dig. Dis. Sci. *50*, 34–38. https://doi.org/10.1007/s10620-005-2804-5.

5. Massier, L., Blüher, M., Kovacs, P., and Chakaroun, R.M. (2021). Impaired Intestinal Barrier and Tissue Bacteria : Pathomechanisms for Metabolic Diseases. Front. Endocrinol. *12*, 1–18. https://doi.org/10.3389/fendo.2021.616506.

6. Fukui, H. (2016). Stomach and Colon : Review Increased Intestinal Permeability and Decreased Barrier Function : Does It Really Influence the Risk of Inflammation ? Inflamm. Intest. Dis. *1*, 135–145. https://doi.org/10.1159/000447252.

7. Sato, T., Vries, R.G., Snippert, H.J., Van De Wetering, M., Barker, N., Stange, D.E., Van Es, J.H., Abo, A., Kujala, P., Peters, P.J., and Clevers, H. (2009). Single Lgr5 stem cells build crypt-villus structures in vitro without a mesenchymal niche. Nature *459*, 262–265. https://doi.org/10.1038/nature07935.

8. Taupin, D., and Podolsky, D.K. (2003). Trefoil factors: Initiators of mucosal healing. Nat. Rev. Mol. Cell Biol. *4*, 721–732. https://doi.org/10.1038/nrm1203.

9. Jung, P., Sato, T., Merlos-Suárez, A., Barriga, F.M., Iglesias, M., Rossell, D., Auer, H., Gallardo, M., Blasco, M.A., Sancho, E., et al. (2011). Isolation and in vitro expansion of human colonic stem cells. Nat. Med. *17*, 1225–1227. https://doi.org/10.1038/nm.2470.

10. Sato, T., and Clevers, H. (2013). Growing self-organizing mini-guts from a single intestinal stem cell: Mechanism and applications. Science *340*, 1190–1194. https://doi.org/10.1126/science.1234852.

11. Barker, N. (2014). Adult intestinal stem cells: Critical drivers of epithelial homeostasis and regeneration. Nat. Rev. Mol. Cell Biol. *15*, 19–33. https://doi.org/10.1038/nrm3721.

12. Donath, S., Angerstein, L., Gentemann, L., Müller, D., Seidler, A.E., Jesinghaus, C., Bleich, A., Heisterkamp, A., Buettner, M., and Kalies, S. (2022). Investigation of Colonic Regeneration via Precise Damage Application Using Femtosecond Laser-Based Nanosurgery. Cells *11*, 1143. https://doi.org/10.3390/cells11071143.

13. Müller, D., Donath, S., Brückner, E.G., Biswanath Devadas, S., Daniel, F., Gentemann, L., Zweigerdt, R., Heisterkamp, A., and Kalies, S.M.K. (2021). How localized z-disc damage affects force generation and gene expression in cardiomyocytes. Bioengineering *8*, 213. https://doi.org/10.3390/bioengineering8120213.

14. Kuetemeyer, K., Rezgui, R., Lubatschowski, H., and Heisterkamp, A. (2010). Influence of laser parameters and staining on femtosecond laser-based intracellular nanosurgery. Biomed. Opt. *1*, 587–597. https://doi.org/10.1364/BOE.1.000587.

15. Vogel, A., Noack, J., Hüttman, G., and Paltauf, G. (2005). Mechanisms of femtosecond laser nanosurgery of cells and tissues. Appl. Phys. B *81*, 1015–1047. https://doi.org/10.1007/s00340-005-2036-6.

16. Watanabe, W., Shimada, T., Itoh, K., Matsunaga, S., and Fukui, K. (2005). Femtosecond laser manipulation of subcellular organelles in living cells. Opt. InfoBase Conf. Pap. *12*, 113–115. https://doi.org/10.1117/12.633079.

17. Karsch, S., Kong, D., Großhans, J., and Janshoff, A. (2017). Single-Cell Defects Cause a Long-Range Mechanical Response in a Confluent Epithelial Cell Layer. Biophys. J. *113*, 2601–2608. https://doi.org/10.1016/j.bpj.2017.10.025.

18. Kuipers, D., Mehonic, A., Kajita, M., Peter, L., Fujita, Y., Duke, T., Charras, G., and Gale, J.E. (2014). Epithelial repair is a two-stage process driven first by dying cells and then by their neighbours. J. Cell Sci. *127*, 1229–1241. https://doi.org/10.1242/jcs.138289.

19. Lacy, E.R. (1988). Epithelial Restitution in the Gastrointestinal Tract. J. Clin. Gastroenterol. *10*, 72–77.

20. Engevik, K.A., Hanyu, H., Matthis, A.L., Zhang, T., Frey, M.R., Oshima, Y., Aihara, E., and Montrose, M.H. (2019). Trefoil factor 2 activation of CXCR4 requires calcium mobilization to drive epithelial repair in gastric organoids. J. Physiol. *597*, 2673–2690. https://doi.org/10.1113/JP277259.

21. Marchiando, A.M., Shen, L., Graham, W.V., Weber, C.R., Schwarz, B.T., Austin, J.R., Raleigh, D.R., Guan, Y., Watson, A.J.M., Montrose, M.H., and Turner, J.R. (2010). Caveolin-1-dependent occludin endocytosis is required for TNF-induced tight junction regulation in vivo. J. Cell Biol. *189*, 111–126. https://doi.org/10.1083/jcb.200902153.

22. Marchiando, A.M., Shen, L., Graham, W.V., Edelblum, K.L., Duckworth, C.A., Guan, Y., Montrose, M.H., Turner, J.R., and Watson, A.J.M. (2011). The epithelial barrier is maintained by in vivo tight junction expansion during pathologic intestinal epithelial shedding. Gastroenterology *140*, 1208–1218.e1-2. https://doi.org/10.1053/j.gastro.2011.01.004.

23. Schindelin, J., Arganda-Carreras, I., Frise, E., Kaynig, V., Longair, M., Pietzsch, T., Preibisch, S., Rueden, C., Saalfeld, S., Schmid, B., et al. (2012). Fiji: An open-source platform for biological-image analysis. Nat. Methods *9*, 676–682. https://doi.org/10.1038/nmeth.2019.

24. Stringer, C., Wang, T., Michaelos, M., and Pachitariu, M. (2021). Cellpose: a generalist algorithm for cellular segmentation. Nat. Methods *18*, 100–106. https://doi.org/10.1038/s41592-020-01018-x.

25. Prevedel, R., Diz-Muñoz, A., Ruocco, G., and Antonacci, G. (2019). Brillouin microscopy: an emerging tool for mechanobiology. Nat. Methods *16*, 969–977. https://doi.org/10.1038/s41592-019-0543-3.

26. Barrasa-Fano, J., Shapeti, A., Jorge-Peñas, Á., Barzegari, M., Sanz-Herrera, J.A., and Van Oosterwyck, H. (2021). TFMLAB: A MATLAB toolbox for 4D traction force microscopy. SoftwareX *15*, 100723. https://doi.org/10.1016/j.softx.2021.100723.

27. Jorge-Peñas, A., Izquierdo-Alvarez, A., Aguilar-Cuenca, R., Vicente-Manzanares, M., Garcia-Aznar, J.M., Van Oosterwyck, H., De-Juan-Pardo, E.M., Ortiz-De-Solorzano, C., and Muñoz-Barrutia, A. (2015). Free form deformation-based image registration improves accuracy of traction force microscopy. PLoS One *10*, 1–13. https://doi.org/10.1371/journal.pone.0144184.

28. Sederberg, T.W., and Parry, S.R. (1986). Free-form deformation of solid geometric models. Proc. 13th Annu. Conf. Comput. Graph. Interact. Tech. SIGGRAPH *20*, 151–160. https://doi.org/10.1145/15922.15903.

29. Aihara, E., Medina-Candelaria, N.M., Hanyu, H., Matthis, A.L., Engevik, K.A., Gurniak, C.B., Witke, W., Turner, J.R., Zhang, T., and Montrose, M.H. (2018). Cell injury triggers actin polymerization to initiate epithelial restitution. J. Cell Sci. *131*, jcs216317. https://doi.org/10.1242/jcs.216317.

30. Levayer, R., and Lecuit, T. (2012). Biomechanical regulation of contractility: Spatial control and dynamics. Trends Cell Biol. *22*, 61–81. https://doi.org/10.1016/j.tcb.2011.10.001.

31. Stricker, J., Falzone, T., and Gardel, M.L. (2010). Mechanics of the F-actin cytoskeleton. J. Biomech. *43*, 9–14. https://doi.org/10.1016/j.jbiomech.2009.09.003.

32. Rottner, K., Faix, J., Bogdan, S., Linder, S., and Kerkhoff, E. (2017). Actin assembly mechanisms at a glance. J. Cell Sci. *130*, 3427–3435. https://doi.org/10.1242/jcs.206433.

33. Blanchoin, L., Boujemaa-Paterski, R., Sykes, C., and Plastino, J. (2014). Actin dynamics, architecture, and mechanics in cell motility. Physiol. Rev. *94*, 235–263. https://doi.org/10.1152/physrev.00018.2013.

34. Tamada, M., Perez, T.D., Nelson, W.J., and Sheetz, M.P. (2007). Two distinct modes of myosin assembly and dynamics during epithelial wound closure. J. Cell Biol. *176*, 27–33. https://doi.org/10.1083/jcb.200609110.

35. Kovács, M., Tóth, J., Hetényi, C., Málnási-Csizmadia, A., and Sellers, J.R. (2004). Mechanism of blebbistatin inhibition of myosin II. J. Biol. Chem. *279*, 35557–35563. https://doi.org/10.1074/jbc.M405319200.

36. Chen, T., Teng, N., Wu, X., Wang, Y., Tang, W., Šamaj, J., Baluška, F., and Lin, J. (2007). Disruption of actin filaments by latrunculin B affects cell wall construction in Picea meyeri pollen tube by disturbing vesicle trafficking. Plant Cell Physiol. *48*, 19–30. https://doi.org/10.1093/pcp/pcl036.

37. Shoji, K., Ohashi, K., Sampei, K., Oikawa, M., and Mizuno, K. (2012). Cytochalasin D acts as an inhibitor of the actin-cofilin interaction. Biochem. Biophys. Res. Commun. *424*, 52–57. https://doi.org/10.1016/j.bbrc.2012.06.063.

38. Aihara, E., and Montrose, M.H. (2014). Importance of Ca2+in gastric epithelial restitution - New views revealed by real-time in vivo measurements. Curr. Opin. Pharmacol. *19*, 76–83. https://doi.org/10.1016/j.coph.2014.07.012.

39. Aihara, E., Hentz, C.L., Korman, A.M., Perry, N.P.J., Prasad, V., Shull, G.E., and Montrose, M.H. (2013). In vivo epithelial wound repair requires mobilization of endogenous intracellular and extracellular calcium. J. Biol. Chem. *288*, 33585–33597. https://doi.org/10.1074/jbc.M113.488098.

40. Rathor, N., Chung, H.K., Song, J.L., Rao, J.N., Wang, S.R., Wang, J.Y., and Rao, J.N. (2021). TRPC1-mediated Ca2+ signaling enhances intestinal epithelial restitution by increasing α4 association with PP2Ac after wounding. Physiol. Rep. *9*, e14864. https://doi.org/10.14814/phy2.14864.

41. Song, H.P., Hou, X.Q., Li, R.Y., Yu, R., Li, X., Zhou, S.N., Huang, H.Y., Cai, X., and Zhou, C. (2017). Atractylenolide I stimulates intestinal epithelial repair through polyamine-mediated Ca2+ signaling pathway. Phytomedicine *28*, 27–35. https://doi.org/10.1016/j.phymed.2017.03.001.

42. Tsai, F.C., Kuo, G.H., Chang, S.W., and Tsai, P.J. (2015). Ca2+ signaling in cytoskeletal reorganization, cell migration, and cancer metastasis. BioMed Res. Int. *2015*, 409245. https://doi.org/10.1155/2015/409245.

43. Russo, J.M., Florian, P., Shen, L., Graham, W.V., Tretiakova, M.S., Gitter, A.H., Mrsny, R.J., and Turner, J.R. (2005). Distinct Temporal-Spatial Roles for Rho Kinase and Myosin Light Chain Kinase in Epithelial Purse-String Wound Closure. Int. J. Obes. *128*, 987–1001.

44. Paupe, V., and Prudent, J. (2018). New insights into the role of mitochondrial calcium homeostasis in cell migration. Biochem. Biophys. Res. Commun. *500*, 75–86. https://doi.org/10.1016/j.bbrc.2017.05.039.

45. Bhatt, A., Kaverina, I., Otey, C., and Huttenlocher, A. (2002). Regulation of focal complex composition and disassembly by the calcium-dependent protease calpain. J. Cell Sci. *115*, 3415–3425. https://doi.org/10.1242/jcs.115.17.3415.

46. Addis, R.C., Ifkovits, J.L., Pinto, F., Kellam, L.D., Esteso, P., Rentschler, S., Christoforou, N., Epstein, J.A., and Gearhart, J.D. (2013). Optimization of direct fibroblast reprogramming to cardiomyocytes using calcium activity as a functional measure of success. J. Mol. Cell. Cardiol. *60*, 97–106. https://doi.org/10.1016/j.yjmcc.2013.04.004.

47. Deng, F., Wu, Z., Zou, F., Wang, S., and Wang, X. (2022). The Hippo–YAP/TAZ Signaling Pathway in Intestinal Self-Renewal and Regeneration After Injury. Front. Cell Dev. Biol. *10*, 894737. https://doi.org/10.3389/fcell.2022.894737.

48. Johnson, R., and Halder, G. (2014). The two faces of Hippo: Targeting the Hippo pathway for regenerative medicine and cancer treatment. Nat. Rev. Drug Discov. *13*, 63–79. https://doi.org/10.1038/nrd4161.

49. Hu, J.K., Du, W., Shelton, S.J., Oldham, M.C., Dipersio, C.M., and Klein, O.D. (2017). An FAK-YAP-mTOR signaling axis regulates stem cell-based tissue renewal in mice. Cell Stem Cell *21*, 91–106. https://doi.org/10.1016/j.stem.2017.03.023.

50. Faix, J., and Rottner, K. (2022). Ena/VASP proteins in cell edge protrusion, migration and adhesion. J. Cell Sci. *135*, jcs259226. https://doi.org/10.1242/jcs.259226.

51. Vasioukhin, V., Bauer, C., Yin, M., and Fuchs, E. (2000). Directed Actin Polymerization Is the Driving Force for Epithelial Cell-Cell Adhesion-catenin associates with several other actin-binding. AJs (Drubin Nelson *100*, 209–219.

52. Grady, M.E., Composto, R.J., and Eckmann, D.M. (2016). Cell elasticity with altered cytoskeletal architectures across multiple cell types. J. Mech. Behav. Biomed. Mater. *61*, 197–207. https://doi.org/10.1016/j.jmbbm.2016.01.022.

53. Christodoulou, N., and Skourides, P.A. (2015). Cell-Autonomous Ca2+ Flashes Elicit Pulsed Contractions of an Apical Actin Network to Drive Apical Constriction during Neural Tube Closure. Cell Rep. *13*, 2189–2202. https://doi.org/10.1016/j.celrep.2015.11.017.

54. Sahu, S.U., Visetsouk, M.R., Garde, R.J., Hennes, L., Kwas, C., and Gutzman, J.H. (2017). Calcium signals drive cell shape changes during zebrafsh midbrain-hindbrain boundary formation. Mol. Biol. Cell *28*, 875–882. https://doi.org/10.1091/mbc.E16-08-0561.

55. Varadarajan, S., Chumki, S.A., Stephenson, R.E., Misterovich, E.R., Wu, J.L., Dudley, C.E., Erofeev, I.S., Goryachev, A.B., and Miller, A.L. (2022). Mechanosensitive calcium flashes promote sustained RhoA activation during tight junction remodeling. J. Cell Biol. *221*, e202105107.

56. Wei, Y., and Li, W. (2021). Calcium, an Emerging Intracellular Messenger for the Hippo Pathway Regulation. Front. Cell Dev. Biol. *9*, 694828. https://doi.org/10.3389/fcell.2021.694828.

57. Azzolin, L., Zanconato, F., Bresolin, S., Forcato, M., Basso, G., Bicciato, S., Cordenonsi, M., and Piccolo, S. (2012). Role of TAZ as mediator of wnt signaling. Cell *151*, 1443–1456. https://doi.org/10.1016/j.cell.2012.11.027.

58. Imajo, M., Miyatake, K., Iimura, A., Miyamoto, A., and Nishida, E. (2012). A molecular mechanism that links Hippo signalling to the inhibition of Wnt/β-catenin signalling. EMBO J. *31*, 1109–1122. https://doi.org/10.1038/emboj.2011.487.

59. Azzolin, L., Panciera, T., Soligo, S., Enzo, E., Bicciato, S., Dupont, S., Bresolin, S., Frasson, C., Basso, G., Guzzardo, V., et al. (2014). YAP/TAZ incorporation in the β-catenin destruction complex orchestrates the Wnt response. Cell *158*, 157–170. https://doi.org/10.1016/j.cell.2014.06.013.

60. Tannenbaum, J., and Bennett, B.T. (2015). Russell and Burch's 3Rs then and now: The need for clarity in definition and purpose. J. Am. Assoc. Lab. Anim. Sci. *54*, 120–132.

61. Balls, M. (2022). Alternatives to Laboratory Animals: Trends in Replacement and the Three Rs. Altern. Lab. Anim. *50*, 10–26. https://doi.org/10.1177/02611929221082250.

62. Pinheiro, D., and Bellaïche, Y. (2018). Mechanical Force-Driven Adherens Junction Remodeling and Epithelial Dynamics. Dev. Cell *47*, 3–19. https://doi.org/10.1016/j.devcel.2018.09.014.

63. Hoffman, B.D., and Yap, A.S. (2015). Towards a Dynamic Understanding of Cadherin-Based Mechanobiology. Trends Cell Biol. *25*, 803–814. https://doi.org/10.1016/j.tcb.2015.09.008.

64. Lecuit, T., and Yap, A.S. (2015). E-cadherin junctions as active mechanical integrators in tissue dynamics. Nat. Cell Biol. *17*, 533–539. https://doi.org/10.1038/ncb3136.

65. Heisenberg, C.P., and Bellaïche, Y. (2013). XForces in tissue morphogenesis and patterning. Cell *153*, 948–962. https://doi.org/10.1016/j.cell.2013.05.008.

66. Pickering, K., Alves-Silva, J., Goberdhan, D., and Millard, T.H. (2013). Par3/Bazooka and phosphoinositides regulate actin protrusion formation during Drosophila dorsal closure and wound healing. Dev *140*, 800–809. https://doi.org/10.1242/dev.089557.

67. Antunes, M., Pereira, T., Cordeiro, J.V., Almeida, L., and Jacinto, A. (2013). Coordinated waves of actomyosin flow and apical cell constriction immediately after wounding. J. Cell Biol. *202*, 365–379. https://doi.org/10.1083/jcb.201211039.

68. Hunter, M.V., Lee, D.M., Harris, T.J.C., and Fernandez-Gonzalez, R. (2015). Polarized E-cadherin endocytosis directs actomyosin remodeling during embryonic wound repair. J. Cell Biol. *210*, 801–816. https://doi.org/10.1083/jcb.201501076.

69. Matsubayashi, Y., Coulson-Gilmer, C., and Millard, T.H. (2015). Endocytosis-dependent coordination of multiple actin regulators is required for wound healing [JCB (2015) 210, 3, 419-433]. J. Cell Biol. *210*, 677–679. https://doi.org/10.1083/jcb.20141103707282015c.

70. Martin, P., and Lewis, J. (1992). Actin cables and epidermalmovement in embryonicwound healing. Nature *360*, 179–183.

71. Brock, J., Midwinter, K., Lewis, J., and Martin, P. (1996). Healing of incisional wounds in the embryonic chick wing bud: Characterization of the actin purse-string and demonstration of a requirement for Rho activation. J. Cell Biol. *135*, 1097–1107. https://doi.org/10.1083/jcb.135.4.1097.

72. Bement, W.M., Mandato, C.A., and Kirsch, M.N. (1999). Wound-induced assembly and closure of an actomyosin purse string in Xenopus oocytes. Curr. Biol. *9*, 579–587. https://doi.org/10.1016/S0960-9822(99)80261-9.

73. Said, R., Wang, H., Pernier, J., Narassimprakash, H., Roméro, S., Gautreau, A.M., Mége, R.-M., and Le Clainche, C. (2022). The adherens junction proteins α-catenin, vinculin and VASP cooperate to promote actin assembly. bioRxiv *33*, 1–12.

74. Breitsprecher, D., Kiesewetter, A.K., Linkner, J., Urbanke, C., Resch, G.P., Small, J.V., and Faix, J. (2008). Clustering of VASP actively drives processive, WH2 domain-mediated actin filament elongation. EMBO J. *27*, 2943–2954. https://doi.org/10.1038/emboj.2008.211.

75. Breitsprecher, D., Kiesewetter, A.K., Linkner, J., Vinzenz, M., Stradal, T.E.B., Small, J.V., Curth, U., Dickinson, R.B., and Faix, J. (2011). Molecular mechanism of Ena/VASP-mediated actin-filament elongation. EMBO J. *30*, 456–467. https://doi.org/10.1038/emboj.2010.348.

76. Clark, A.G., Miller, A.L., Vaughan, E., Yu, H.Y.E., Penkert, R., and Bement, W.M. (2009). Integration of Single and Multicellular Wound

Responses. Curr. Biol. *19*, 1389–1395. https://doi.org/10.1016/j.cub.2009.06.044.

77. Florian, P., Schöneberg, T., Schulzke, J.D., Fromm, M., and Gitter, A.H. (2002). Single-cell epithelial defects close rapidly by an actinomyosin purse string mechanism with functional tight junctions. J. Physiol. *545*, 485–499. https://doi.org/10.1113/jphysiol.2002.031161.

78. Pentinmikko, N., Lozano, R., Scharaw, S., Andersson, S., Englund, J.I., Castillo-Azofeifa, D., Gallagher, A., Broberg, M., Song, K.Y., Sola Carvajal, A., et al. (2022). Cellular shape reinforces niche to stem cell signaling in the small intestine. Sci. Adv. *8*. eabm1847-13. https://doi.org/10.1126/sciadv.abm1847.

79. Engevik, K.A., Karns, R.A., Oshima, Y., and Montrose, M.H. (2020). Multiple calcium sources are required for intracellular calcium mobilization during gastric organoid epithelial repair. Physiol. Rep. *8*, e14384. https://doi.org/10.14814/phy2.14384.

80. Chaoliang, W., Xianhua, W., Min, C., Kunfu, O., Long-Sheng, S., and Cheng, H. (2008). Calcium Flickers Steer Cell Migration. Nature *23*, 1–7. https://doi.org/10.1038/nature07577.Calcium.

81. Kühl, M., Sheldahl, L.C., Malbon, C.C., and Moon, R.T. (2000). Ca2+/calmodulin-dependent protein kinase II is stimulated by Wnt and Frizzled homologs and promotes ventral cell fates in Xenopus. J. Biol. Chem. *275*, 12701–12711. https://doi.org/10.1074/jbc.275.17.12701.

82. Piccolo, S., Dupont, S., and Cordenonsi, M. (2014). The biology of YAP/TAZ: Hippo signaling and beyond. Physiol. Rev. *94*, 1287–1312. https://doi.org/10.1152/physrev.00005.2014.

83. Zhou, D., Zhang, Y., Wu, H., Barry, E., Yin, Y., Lawrence, E., Dawson, D., Willis, J.E., Markowitz, S.D., Camargo, F.D., and Avruch, J. (2011). Mst1 and Mst2 protein kinases restrain intestinal stem cell proliferation and colonic tumorigenesis by inhibition of Yes-associated protein (Yap) overabundance. Proc. Natl. Acad. Sci. USA *108*, E1312–E1320. https://doi.org/10.1073/pnas.1110428108.

84. Barry, E.R., Morikawa, T., Butler, B.L., Shrestha, K., De La Rosa, R., Yan, K.S., Fuchs, C.S., Magness, S.T., Smits, R., Ogino, S., et al. (2013). Restriction of intestinal stem cell expansion and the regenerative response by YAP. Nature *493*, 106–110. https://doi.org/10.1038/nature11693.

85. Mueller, J., Dimchev, G., Schaks, M., Nemethova, M., Pokrant, T., Bru, S., Linkner, J., Blanchoin, L., Sixt, M., Rottner, K., et al. (2020). Loss of Ena/VASP Interferes with Lamellipodium Architecture , Motility and Integrin-dependent Adhesion, pp. 1–31.

86. Mahe, M.M., Aihara, E., Schumacher, M.A., Zavros, Y., Montrose, M.H., Helmrath, M.A., Sato, T., and Shroyer, N.F. (2013). Establishment of Gastrointestinal Epithelial Organoids. Curr. Protoc. Mouse Biol. *3*, 217–240. https://doi.org/10.1002/9780470942390.mo130179.

87. Schambach, A., Galla, M., Modlich, U., Will, E., Chandra, S., Reeves, L., Colbert, M., Williams, D.A., von Kalle, C., and Baum, C. (2006). Lentiviral vectors pseudotyped with murine ecotropic envelope: Increased biosafety and convenience in preclinical research. Exp. Hematol. *34*, 588–592. https://doi.org/10.1016/j.exphem.2006.02.005.

88. De Van Lidth Jeude, J.F., Vermeulen, J.L.M., Montenegro-Miranda, P.S., Van Den Brink, G.R., and Heijmans, J. (2015). A protocol for lentiviral transduction and downstream analysis of intestinal organoids. J. Vis. Exp. *2015*, 52531. https://doi.org/10.3791/52531.

89. Müller, D., Hagenah, D., Biswanath, S., Coffee, M., Kampmann, A., Zweigerdt, R., Heisterkamp, A., and Kalies, S.M.K. (2019). Femtosecond laser-based nanosurgery reveals the endogenous regeneration of single Z-discs including physiological consequences for cardiomyocytes. Sci. Rep. *9*, 1–10. https://doi.org/10.1038/s41598-019-40308-z.

90. Wenzel, J., Ruprich, N., Sperlich, K., Stachs, O., Schunemann, M., Leyh, C., Kalies, S., and Heisterkamp, A. (2022). Non-Invasive Full Rheological Characterization via Combined Speckle and Brillouin Microscopy. IEEE Access *10*, 75527–75535. https://doi.org/10.1109/ACCESS.2022.3192463.

91. Sanz-Herrera, J.A., Barrasa-Fano, J., Cóndor, M., and Van Oosterwyck, H. (2021). Inverse method based on 3D nonlinear physically constrained minimisation in the framework of traction force microscopy. Soft Matter *17*, 10210–10222. https://doi.org/10.1039/d0sm00789g.

92. Steinwachs, J., Metzner, C., Skodzek, K., Lang, N., Thievessen, I., Mark, C., Münster, S., Aifantis, K.E., and Fabry, B. (2016). Three-dimensional force microscopy of cells in biopolymer networks. Nat. Methods *13*, 171–176. https://doi.org/10.1038/nmeth.3685.

STAR★METHODS

KEY RESOURCES TABLE

REAGENT or RESOURCE	SOURCE	IDENTIFIER
Antibodies		
Mouse monoclonal anti-YAP1	DSHB	Cat# YAP1 8J19; RRID:AB_2619554
Rabbit monoclonal anti-VASP	Mueller et al.[85]	N/A
AlexaFluor® 647 Donkey anti-rabbit IgG	Biolegend	Cat# 406414; AB_2563202
AlexaFluor™ 647 goat anti-mouse IgG	Invitrogen	Cat# A-21235; AB_2535804
Bacterial and virus strains		
NEB® 10-beta compotent E. *coli* (High Efficiency)	NEB	Cat# C3019I
pLV-CMV-Occludin-mEmerald-G418	This Paper	N/A
pLV-GCamp5-Blast	This Paper	N/A
Biological samples		
Murine colonic tissue	Medical School Hannover, ZTL	N/A
Chemicals, peptides, and recombinant proteins		
DPBS	Sigma-Aldrich	Cat# D8537
EDTA	Carl Roth	Cat# CN06.3
Sorbitol	Carl Roth	Cat# 6213.1
Sucrose	Carl Roth	Cat# 4661.1
N-2 Supplement	Invitrogen	Cat# 17502048
B27™ Supplement	Invitrogen	Cat# 17504044
EGF	Sigma-Aldrich	Cat# E5160
Y-27632	Hoelzel-Biotech	Cat# HY-10583
Polybren	Bio-Techne	Cat# 7711/10
TrypLE Select	Thermo Fisher	Cat# 12563011
Chir99021	Hoelzel-Biotech	Cat# USB-C4137
Paraformaldehyd	Sigma-Aldrich	Cat# 158127
Glycin	Carl Roth	Cat# 3790.1
Blebbistatin	Sigma-Aldrich	Cat# B0560
Latrunculin B	Sigma-Aldrich	Cat# L5288
Cytochalasin D	Sigma-Aldrich	Cat# C8273
Experimental models: Cell lines		
HEK293T	DSMZ	Cat# ACC 635
L-WRN	ATCC	CRL-3276™
Recombinant DNA		
Plasmid: Occludin-mEmerald-G418	This Paper	N/A
Plasmid: GCamp5-Blast	This Paper	N/A
Software and algorithms		
ImageJ	Schneider et al.[23]	https://imagej.nih.gov/ij/
Cellpose	Stinger et al.[24]	https://github.com/MouseLand/cellpose
OriginPro 2019	Origin Lab Corp.	https://www.originlab.com/
TFMLab	Barrasa-Fano et al.[26]	https://github.com/ElsevierSoftwareX/SOFTX-D-20-00104
MATLAB	Math Works	https://www.mathworks.com/products/matlab.html

Continued

REAGENT or RESOURCE	SOURCE	IDENTIFIER
Other		
Latex beads, sulfate-modified polystyrene, fluorescent red	Sigma-Aldrich	Cat# L9902
Cultrex Reduced Growth Factor Basement Membrane Extract (BME), Type R1	Bio-Techne	Cat 3433-010-R1
Phalloidin-Atto 488	Sigma-Aldrich	Cat# 49409
Helix NP™ Blue	Biolegend	Cat# 425305
DMEM, high glucose	Sigma-Aldrich	Cat# D6429
DMEM, high glucose, GlutaMAX™ Supplement, pyruvate	Thermo Fisher	Cat# 31966021
FCS	Sigma-Aldrich	Cat# F7524
BSA	Sigma-Aldrich	Cat# A7030
BAPTA-AM	Sigma-Aldrich	Cat# A1076
Triton™ X-100	Sigma-Aldrich	Cat# X-100

RESOURCE AVAILABILITY

Lead contact

Further information and requests for resources and reagents should be directed to and will be fulfilled by the lead contact, Stefan Kalies (kalies@iqo.uni-hannover.de).

Materials aviability

Materials, which were generated in this study are available upon request. Please contact lead contact, Dr. Kalies.

Data and code aviability

- All data reported in this paper will be shared by the lead contact upon request.
- This paper does not report original code.
- Any additional information required to reanalyze the data reported in this paper is available from the lead contact upon request.

EXPERIMENTAL MODEL AND STUDY PARTICIPANT DETAILS

Isolation of colonic crypts and growth of colonoids

The protocol for the isolation of murine colonic crypts for the preparation of colonoids was based on the work of Mahe et al.[86] The experiments complied with the German Animal Protection Act (§4, TierSchG) and were approved by the local institutional advisory committee for animal care and research and by the Lower Saxony State Office for Consumer Protection and Food Safety (file number 42500/1H).

Mice at the age of 6–14 weeks independent of sexes were anesthetized with an overdose of CO_2. After the absence of the middle toe reflex, cervical-dislocation was performed. The abdomen of the mouse was opened, and the colon was removed and transferred to a sterile environment in 4°C cooled Dulbecco's phosphate-buffered saline (DPBS, Sigma-Aldrich, St. Louis, MO, USA) without calcium and magnesium. Fat strands leading laterally along the colon were removed, the colon was irrigated externally and internally and cut open laterally. The colon was cut into 2 mm pieces, which were transferred to 4°C chelation buffer (CCB, DPBS, 2 mM EDTA, Carl Roth, Karlsruhe, Germany) and rotated slowly in ice for 30 min. Afterward, the chelated crypts were washed twice with CCB and transferred to 5 mL dissection buffer (DB, DPBS, 54.9 mM sorbitol, and 43.4 mM sucrose, Carl Roth). The crypts were shaken vigorously by hand for 7 min. The detached colonic crypts were filtered (70 μm) and the used tube and the filter were washed with 10 mL DB. The suspension was centrifuged at 500 rcf and 4°C for 10 min. The supernatant was removed and the pellet of detached crypts was resuspended a second time in 5 mL DB for washing and centrifuged at 750 rcf at 4°C for 10 min. Depending on the size of the pellet of extracted crypts, 700–1000 μL of Cultrex Reduced Growth Factor Basement Membrane Extract (BME), Type R1 (R&D Systems, Minneapolis, MN, USA) was added. The suspension was plated out in 30 μL drops in a 24-well plate (Costar Cell Culture Plate, Corning Incorporate, New York, NY, USA) preheated to 37°C. The BME was allowed to solidify at 37°C and 5% CO_2 for 30 min. Crypts were then cultured with 500 μL conditioned organoid growth medium, composed of DMEM, high glucose, GlutaMAX, pyruvate (Thermo Fisher Scientific, Massachusetts, MA, USA) with 50% L-WRN-supernatant (ATCC CRL3276 in DMEM, high glucose, GlutaMAX, pyruvate plus 10% fetal calf serum), 1x N2 (Invitrogen, Carlsbad, CA, USA), 1x B27 (Invitrogen), 50 ng/μL recombinant mouse epidermal growth factor (EGF, Sigma-Aldrich), 10 μM Y-27632 (Tocris, Bristol, UK), and 1x Cellshield (Biochrom, Berlin, Germany) and grown at 37°C and 5% CO_2.

The experiments were in accordance with the German Animal Welfare Legislation (§4, TierSchG), approved by the local Institutional Animal Care and Research Advisory Committee, and permitted by the Lower Saxony State Office for Consumer Protection and Food Safety (reference number 42500/1H).

METHOD DETAILS

Colonoid culture and transduction

The isolated colonic crypts were split approximately ten days after isolation. In the first seven days after isolation and after transduction, the concentration of the ROCK inhibitor Y-27632 was increased from 10 μM to 20 μM. The colonoids were used for transduction three passages after isolation. The lentiviral vectors were produced via a third-generation split packaging protocol in 293T cells (DSMZ, Braunschweig, Germany), as previously described.[87] One of the two transfer plasmids used contained the sequence for expression of the fusion protein of occludin and mEmerald under the control of a CMV promoter. The second plasmid utilized the GCaMP5 sequence in the lentiviral backbone, indicating calcium signaling via the fluorescence of GFP.[46]

The transduction protocol is based on Lidth de Jeude's procedure.[88] Here, 8 μg/mL polybrene (R&D Systems) was added to the medium 2 h before the start of transduction. The BME and four moderately dense wells of colonoids were disrupted at the beginning of the transduction, centrifuged (750 rcf, 4°C, 5 min), and then dissociated into single cells by digestion with TrypLE Select (Thermo Fisher Scientific) for 10 min at 37 C. During that incubation period, the colonoids were resuspended using a 1000 μL pipette at 2-min intervals and, in the final step, aspirated and withdrawn through a 24G cannula. The dissociated colonoids were centrifuged (850 rcf, RT, 5 min) and resuspended using 1.25 mL of conditioned colonoid growth medium containing 8 μg/mL polybrene, 100 ng/mL EGF and 2.5 μM CHIR99021 (Hölzel Diagnostika, Cologne, Germany). The resuspended cells were transferred into a 2 mL SafeSeal tube previously coated with 0.1% BSA (Sigma Aldrich). Afterward, 250 μL of the respective lentivirus ($2*10^7$ IU) was added to the cells. The cell suspension was rotated at 4°C with 20 rotations per minute. After 3 h, the cells were carefully resuspended using a 1000 μL pipette. After 6h rotation, the cells were centrifuged at 850 rcf and 4°C for 5 min, the pellet was taken up in 100 μL BME and plated on two Ibidi glass bottom dishes (μ-Dish 35 mm, high Grid-500 Glass, Ibidi, Graefelfing, Germany). The BME was allowed to solidify at 37°C and 5% CO_2 for 30 min. Crypts were then cultured with 1.5 mL conditioned colonoid growth medium with a concentration of 20 μM Y-27632, as described above.

Nanosurgery setup, manipulation, and imaging of colonoids

Imaging of colonoids was performed using a Leica TCS SP5 confocal laser scanning microscope (Leica Microsystems, Wetzlar, Germany). Z-stacks were recorded using a 25x/0.9 water-immersion objective (Leica Microsystems) with an NA of 0.9 and an axial resolution of 2 μm. All acquired images were analyzed using Fiji/ImageJ.[23] For cell ablation and visualization during ablation (multiphoton microscopy) a Chameleon Ultra II laser system (Coherent Inc., Santa Clara, CA, USA) with a pulse length of 140 fs and a repetition rate of 80 MHz was used. The setup was described previously.[12,13,89] The laser beam was focused into the sample via a 40x/1.2 water immersion objective. A wavelength of 730 nm, a pulse energy of 0.9 nJ, and a dissection speed of 15 μm/s were used for single-cell ablation. The parameters used were validated in a previous study.[12]

During multiphoton imaging, the labeled colonoids were visualized using an excitation wavelength of 730 nm (autofluorescence) or 900 nm (mEmerald/GFP) with a power of 100 mW. The emission of NADH-based autofluorescence of the colonoids was recorded at 460 ± 20 nm and the emission of mEmerald/GFP was recorded at 510–560 nm using a photomultiplier tube (Hamamatsu Photonics, Shizuoka, Japan).

Analysis of cell morphology

The analysis of cell morphology was performed in colonoids expressing Occludin-mEmerald. As we were interested in the cell area, perimeter, and aspect ratio, Cellpose was used for 2D cell segmentation.[24] Cellpose is a highly pre-trained deep learning-based cell segmentation method, which enables manual labeling and revision of the automatically generated results. The recorded stacks were split into planes, which were used afterward to further train the pre-trained model. The segmented label images were transferred to ImageJ/Fiji and converted to images with regions of interest (ROIs) using a self-written ImageJ macro. This macro also determined the size of the cell, the perimeter, and the cellular aspect ratio. The data of the different ROIs were then summarized depending on the two-dimensional distance of the ROI from the ablation site, which was set within the macro (0, 20, 40, 60, 80, 100 μm) and analyzed via OriginPro 2019 (OriginLab Corporation, Northampton, MA, USA). For statistical analysis, a t-test was performed between the individual time points within the respective distances from the ablation site. In all cases, p values ≤0.05 were considered statistically significant.For visualization, the individual cells from different planes were projected via z-projection.

Optical elastography via Brillouin microscopy

We evaluated the longitudinal modulus of the colonoids via Brillouin microscopy using a home-built setup that was described previously.[90] Firstly, general morphology was assessed using a transmitted light microscope. For the Brillouin measurements, the colonoids stayed in colonoid growth medium and were imaged using a 10x/0.28 objective (M Plan Apo, Edmund Optics Inc., Barrington, NJ, US). A selected crypt was refined with the help of a halogen lamp in transmitted light mode and settled manually with a translation table. The crypts were scanned using a laser power of 8 mW at a wavelength of 780 nm over a range of 130 μm × 130 μm with a step size of 6.5 μm. At every point, the

integration time for the Brillouin shift was 1–2 s and the signals were analyzed using a VIPA spectrometer. The Brillouin spectrum of water (5.12 GHz) was used as a reference and the Brillouin shift of every point was determined and analyzed using a self-written MATLAB code.[90]

The crypts were measured directly before the laser process, and 30 min, 45 min, 60 min, 120 min, and 240 min after laser ablation. Between the measurement, the colonoids were stored in the incubator at 37°C and 5% CO_2.

Traction force microscopy

To quantify the exerted forces, 1 μm fluorescent beads (Sigma Aldrich) were added to the basement membrane at a dilution of 1:100. A single cell was ablated according to the manipulation section and visualized subsequently using a Leica SP5 confocal microscope. The acquired images were drift corrected, cropped, and filtered in ImageJ[23] before Traction Force Microscopy was performed using the MATLAB toolbox TFMLAB by Barrasa-Fano et al.[26] This software calculates the bead displacements with the Free-Form Deformation (FFD) method and reconstructs the forces applied in three dimensions and over multiple time steps via a physically-based nonlinear inverse method (PBNIM).[26,91] An external Finite Elemente-solver, Abaqus (Dassault Systèmes, Vélizy-Villacoublay, France), was used.

For the displacement calculation, the parameters suggested by Barrasa-Fano et al.[26] were used. For force reconstruction, pre-smoothing of 1, an element cell size of 2, an element ECM of 200, 2 repeats of iterative smoothing, and lowpass smoothing with a value of 0.3 were selected. For the mechanical parameters of the BME, beads as displacement field markers, an elastic modulus of 394 Pa, and a Poission's ratio of 0.25 were specified. The used properties of the basement membrane extract were from the supplementary notes of Steinwachs et al. (2016)[92]; assuming that Cultrex R1 (R&D Systems), which is used here, behaves similarly enough to Matrigel (Corning, New York, USA) to use these values. Steinwachs et al. (2016)[92] assume an approximately linear behavior of the basement membrane matrix, which was also used in our calculation. The output of TFMLAB was filtered using MATLAB (removal of falsely computed forces at edge planes) and visualized in ParaView and MATLAB for further analysis.

Immunostaining

To investigate epithelial restitution and following repair in the crypt base of the colonoids, a single cell was ablated using the femtosecond laser. 60 min after ablation, the colonoids were fixed using pre-cooled 4% paraformaldehyde (PFA, Sigma Aldrich) for 60 min at 4°C. Subsequently, the colonoids were washed three times for 20 min with DPBS. After washing, the colonoids were permeabilized with 0.5% Triton X-(Sigma Aldrich) in DPBS containing 125 mM glycine (Carl Roth). This was followed by blocking using 5% FCS (Sigma Aldrich) in DPBS. The primary antibodies were used in different dilutions in the blocking solution (5% FCS in DPBS). Incubation of the primary antibodies was done for 1 h at RT whilegently shaking. After this incubation period, the colonoids were incubated with the primary antibody at 4°C overnight. The colonoids were then washed three times with DPBS for 20 min and incubated with the secondary antibody for 20–24 h. After the complete staining procedure, the colonoids were washed and visualized on a Leica TCS SP5 confocal laser scanning microscope. In detail, the following primary antibodies were used: mouse anti-YAP1 (DSHB, Iowa, USA, 57 μg/mL, used 1:10), rabbit anti-VASP[85] (gift from Prof. Jan Faix, MHH, Hannover, Germany, used 1:100). For visualization the following secondary antibodies were used: AlexaFluor 647 Donkey anti-rabbit IgG (Biolegend, San Diego, CA, USA) and AlexaFluor 647 goat anti-mouse IgG (Invitrogen).

QUANTIFICATION AND STATISTICAL ANALYSIS

For statistical analysis, a t-test was performed. Data are shown as mean values with error bars, which indicate ±SEM. Detailed information as number of experiments and significance are shown in the figures and figure legends.